



CHORUS

This is the accepted manuscript made available via CHORUS. The article has been published as:

Time-optimal control by a quantum actuator

Clarice D. Aiello and Paola Cappellaro

Phys. Rev. A **91**, 042340 — Published 30 April 2015

DOI: [10.1103/PhysRevA.91.042340](https://doi.org/10.1103/PhysRevA.91.042340)

Time-optimal control by a quantum actuator

Clarice D. Aiello¹ and Paola Cappellaro^{2,*}

¹*Department of Electrical Engineering and Computer Science,*

²*Department of Nuclear Science and Engineering and Research Laboratory of Electronics,
Massachusetts Institute of Technology, Cambridge, MA, USA*

Indirect control of qubits by a quantum actuator has been proposed as an appealing strategy to manipulate qubits that couple only weakly to external fields. While universal quantum control can be easily achieved when the actuator-qubit coupling is anisotropic, the efficiency of this approach is less clear. Here we analyze the time-efficiency of quantum actuator control. We describe a strategy to find time-optimal control sequence by the quantum actuator and compare their gate times with direct driving, identifying regimes where the actuator control performs faster. As a paradigmatic example, we focus on a specific implementation based on the Nitrogen-Vacancy center electronic spin in diamond (the actuator) and nearby carbon-13 nuclear spins (the qubits).

PACS numbers: 03.65.Vf, 61.72.jn, 06.30.Gv

Fast and high fidelity control of quantum systems is a key ingredient for quantum computation and sensing devices. The critical task is to reliably control a quantum system, while staving off decoherence, by keeping it isolated from any external influence. These requirements pose a contradiction: fast control implies a strong coupling to an external controlling system, but this entails an undesired interaction with the environment, leading to decoherence. One is then often faced with the choice between using a strongly connected system, implying a stronger noise, or a weakly connected one, which is more isolated from the environment and thus offers longer coherence times, but results in slower control. A strategy to overcome these issues is to use a hybrid system where a quantum actuator interfaces the quantum system of interest to the classical controller, thus allowing fast operations while preserving the system isolation and coherence [1]. This strategy has been proposed for a broad range of systems, from superconducting qubits [2, 3] to nanomechanical resonator [4, 5] and qubit networks [6, 7]. This indirect control is particularly appropriate for nuclear spin qubits, which only couple weakly to external fields, but often show strong interactions with nearby electronic spins. This model describes several systems, from spins associated with phosphorus donors in Si [8], to fullurene qubits [9], ensemble-ESR systems (such as malonic acid [10]) and, most recently, Nitrogen-Vacancy (NV) centers in diamond [11, 12]. While there are practical advantages to this indirect control strategy, as it does not require experimental apparatus to directly drive the nuclear spins, an important question is whether it can reach faster manipulation than direct control. In this letter we describe a strategy to achieve time-optimal indirect control of a qubit by a two-level quantum actuator. We focus on the NV center in diamond as a paradigmatic example, assessing the achievable gate times of this strategy as compared with those for direct driving. The methods and results are however broader: thanks to the wide

range of couplings to ¹³C spins in the lattice, we can survey a large parameter space, encompassing many other physical systems considered as qubit candidates.

We propose to use alternating controls to drive the evolution of a nuclear spin anisotropically hyperfine-coupled to an electronic spin [10, 13]; in particular, periodically driving the spin of a NV center in diamond can steer the evolution of a proximal ¹³C nuclear spin in a potentially shorter time than a direct, slow radio-frequency (rf) addressing. In general, the method ensures the use of the nuclear spin as a resource within the same implementation time range of direct addressing, while entirely by-passing the application of rf, thus avoiding any noise and errors associated with it [14].

The paper is organized as follow. We first introduce the general concepts of control by a quantum actuator, using the NV center spin system to provide a concrete physical example. We then show how to find the time-optimal actuator control sequence, combining algebraic constraints with numerical optimization. The main results of the paper are an extended comparison of the quantum actuator control with direct driving of the qubit. We use the NV center spin system to explore a broad range of parameters in order to show when actuator control is more convenient, ending the paper with a discussion of more general applications. Some technical results are contained in the appendices.

I. QUANTUM ACTUATOR

A. Indirect control by a quantum actuator

We assume a two-level quantum actuator, with eigenstates $|0\rangle, |1\rangle$ separated by an energy gap much larger than the coupling to the qubit; then, the qubit Hamiltonian depends on the state of the quantum actuator:

$$\mathcal{H} = \mathcal{H}_a + \mathcal{H}_q + |0\rangle\langle 0|_a \otimes \mathcal{H}_q^0 + |1\rangle\langle 1|_a \otimes \mathcal{H}_q^1, \quad (1)$$

where $\mathcal{H}_{a,q}$ are the internal Hamiltonian of the actuator and qubit, respectively, and we only retained the part

* pcappell@mit.edu

of the coupling Hamiltonian that conserves the actuator eigenstates. The qubit thus evolves under two different Hamiltonians depending on the actuator state. Switching between the actuator eigenstates is enough to achieve full controllability of the qubit, as long as the coupling is anisotropic [10, 13]. In the absence of direct driving of the qubit, Pontryagin's minimum principle proves that this bang-bang control achieves time-optimality [15–17].

As a concrete example, we consider a single NV center electronic spin $S = 1$ [18, 19] coupled to a ^{13}C nuclear spin $I = 1/2$ [20, 21] (see Appendix A). Their Hamiltonian is

$$\mathcal{H} = \Delta S_z^2 + \gamma_e B_0 S_z + \gamma_C B_0 I_z + \vec{S} \cdot \mathbf{A} \cdot \vec{I}, \quad (2)$$

where $\Delta = 2.87\text{GHz}$ is the NV zero-field splitting; $\gamma_e \approx 2.8\text{MHz/G}$, $\gamma_C \approx 1\text{kHz/G}$ are, respectively, the gyromagnetic ratios of the electron and nuclear spins; B_0 is a static magnetic field along the NV \hat{z} -axis; and \mathbf{A} is the hyperfine tensor. The NV spin triplet can be reduced to an effective two-level system by driving the system on resonance with a transition between two S_z eigenstates (e.g. $|m_s = 0\rangle \leftrightarrow |m_s = +1\rangle$), while the third eigenstate (e.g. $|m_s = -1\rangle$) can be neglected. Then the Hamiltonian can be rewritten in the electronic spin rotating frame as

$$\mathcal{H} = \omega_0 I_z + S_z \vec{A}_z \cdot \vec{I} = |0\rangle\langle 0| \omega_0 I_z + |\pm 1\rangle\langle \pm 1| (\omega_0 I_z \pm \vec{A}_z \cdot \vec{I}), \quad (3)$$

where $\omega_0 = \gamma_C B_0$ (that we assume > 0). The contact and dipolar contributions [21] to the hyperfine coupling \vec{A} can be described by a longitudinal component A_{\parallel} and a transverse component A_{\perp} , that we will take without loss of generality along the \hat{x} direction. The nuclear spin thus rotates around two distinct axes, depending on the electronic spin manifold. Then, a simple strategy for the indirect control of the nuclear spin is to induce alternating rotations by flipping the electronic spin state with (fast) π -pulses. We define the axes and rotation speeds in the two manifolds as

$$\omega_{\pm} = \gamma_C B_0 = \kappa \omega_{\pm 1}, \quad \omega_{\pm 1} = \sqrt{(\omega_0 \pm A_{\parallel})^2 + A_{\perp}^2}, \quad (4)$$

$$\hat{v}_0 = \hat{z}, \quad \hat{v}_{\pm 1} = \hat{z} \cos(\alpha) + \hat{x} \sin(\alpha),$$

with

$$\tan(\alpha) = \frac{A_{\perp}}{\omega_0 \pm A_{\parallel}}, \quad \kappa = \frac{\omega_0}{\omega_{\pm 1}}. \quad (5)$$

If the NV electronic spin is initially in the $|0\rangle$ state, applying π -pulses at times T_k gives the nuclear spin evolution:

$$U = e^{-i\phi_n^1 \vec{v}_1 \cdot \vec{\sigma}} \dots e^{-i\phi_0^0 \vec{v}_0 \cdot \vec{\sigma}} e^{-i\phi_{k-1}^1 \vec{v}_1 \cdot \vec{\sigma}} \dots e^{-i\phi_0^0 \vec{v}_0 \cdot \vec{\sigma}}, \quad (6)$$

where $\phi_k^{0(1)} = (T_k - T_{k-1})\omega_{0(1)}$, for odd (even) k , and $\vec{\sigma}$ are the Pauli matrices.

B. Time-optimal control by a quantum actuator

For a fair comparison to direct driving, we need to consider the time-optimal synthesis of the desired unitary

U by alternating rotations [15, 16, 22]. Explicit solutions to this optimization problem have been recently obtained using algebraic methods [22, 23] and we only describe here the most important and relevant results.

The optimization of Eq. (6) looks daunting at first, since one needs to find $n \leq \infty$ phases ϕ_k . However, it was found [15, 22] that for $n \geq 4$, the internal angles are related by

$$\tan\left(\frac{\phi^1}{2}\right) = \tan\left(\frac{\phi^0}{2}\right) \frac{\kappa - \cos(\alpha)}{1 - \kappa \cos(\alpha)}, \quad (7)$$

with $\phi^1(\phi^0)$ the rotation angle about $\vec{v}_1(\vec{v}_0)$. Thus the solution depends on only four parameters, greatly simplifying the problem: the outer angles ϕ_i, ϕ_f , the internal angle ϕ^0 of the rotation around \vec{v}_0 , and the total number of rotations n (the sequence length). We can distinguish two important cases that yield different time-optimal solutions, whether $\kappa \leq \cos(\alpha)$. This condition is simply set by the sign of the longitudinal hyperfine interaction, since it corresponds to $\omega_0 \leq (\omega_0 \pm A_{\parallel})$.

If $\kappa < \cos(\alpha)$, optimal sequences are finite and we always have $\phi_0 \leq \pi$ and $\phi_1 \geq \pi$. Finite sequences with $n \geq 6$ have $\pi/3 < \phi_0 < \pi$ and their length is bound by $n \leq \lfloor \frac{2\pi}{\alpha} \rfloor + 1$.

For $\kappa > \cos(\alpha)$, both finite and infinite time-optimal sequences are possible. For large angles between rotation axes, $\alpha > 2\pi/3$, only $n = 3$ or infinite sequences are possible, with $\phi_0 > \pi$. For smaller angles, we can have longer time-optimal sequences. The number of switches is limited by $n \leq \lfloor \frac{\pi}{\alpha} \rfloor + 3$ and, correspondingly, we have $\pi < \phi_0 \leq \frac{(n-1)}{(n-2)}\pi$. Loose bounds can also be found for the outer angles [23] and thus on the total time to implement general unitaries.

These conditions on the admissible time-optimal sequences severely constraint the search space of the time-optimal control sequence for specific goal unitaries and Hamiltonian parameters. We were thus able to perform an exhaustive analysis of time-optimal control for a large number of nuclear spins surrounding the NV center. In turns, the broad range of parameters considered allows us to encompass many other physical situations, also not linked with the specific system considered here.

II. COMPARISON WITH DIRECT DRIVING

An alternative strategy for qubit control is to use classical driving fields. Resonant driving along a desired rotation axis achieves time-optimal steering of the qubit in the xy plane [15, 24].

Even when the direct driving of the qubit is slow, the rate might be increased by virtual transition of the actuator. This is the case for nuclear spins: while their coupling to an external driving field is weak, indirect forbidden transitions mediated by the electronic spin can considerably enhance the driving strength [20, 25, 26]. This nuclear Rabi enhancement depends on the state of

the electronic spin. The effective Rabi frequency Ω for an isolated nuclear spin, hence, is modified from its bare value $\bar{\Omega}$ by the enhancement factors $\zeta_{0,\pm 1}$, corresponding to the electronic spin states $|0\rangle, |\pm 1\rangle$ (see Appendix B). The enhancement is proportional to the ratio of the qubit and actuator coupling to the external field. For nuclear and electronic spins considered here, $\gamma_e/\gamma_n \approx 2600$ and the effective Rabi frequencies $\Omega_i = (1 + \zeta_i)\bar{\Omega}$ can be much larger than the bare frequency.

We assume $\bar{\Omega} \approx 100\text{kHz}$ as an upper-limit on realistic bare nuclear Rabi frequencies by considering data in [27], where the ^{13}C considered was only weakly coupled and thus no Rabi enhancement was present. To achieve this strong driving, a dedicated microfabricated coil was necessary [28]. Rabi frequencies $\bar{\Omega} \approx 20\text{kHz}$ are, in our experience, in the upper achievable range with modest amplifiers and a simple wire to deliver the rf field.

Both regimes of $\kappa \leq \cos(\alpha)$ for the time-optimal solutions can be explored in the NV center system by considering the coupling to ^{13}C at different distances from the NV defect [29–31]. The hyperfine tensors for ^{13}C located up to $\approx 8\text{\AA}$ away from the NV center were estimated using density functional theory [32]. In what follows, we numerically compare the performance of the proposed control method against direct driving under diverse experimental conditions and for a number of distinct nuclear spins.

Using the relationship between internal angles given by Eq. (7) and the bounds on their values, we numerically searched for sequences U^* , by solving the numerical equations for the 3 angle parameters. The search was deemed successful when the fidelity $F \equiv \frac{1}{2}|\text{tr}(U^*U_{\text{goal}}^\dagger)| = 1 - \epsilon$, with $\epsilon \lesssim 10^{-10}$. We repeat the search for different sequence lengths and choose the sequence with minimal time cost among all sequences obtained in successful searches to ensure that we are at the global time-optimum within numerical error.

Typical results for the case $\kappa < \cos(\alpha)$ are illustrated in Fig. (1) by a ^{13}C at a distance $r \approx 2.92\text{\AA}$ from the NV center, at an external magnetic field $B_0 \approx 500\text{G}$ ($\omega_0 = 0.5\text{MHz}$) aligned with the \hat{z} axis. This magnetic field strength is experimentally convenient: it achieves fast nuclear spin polarization since in the electronic excited state the nuclear and electronic spins have similar energies, allowing polarization transfer during optical illumination. We will consider later the effects of different magnetic field strengths. The hyperfine interaction of this spin, $A_{\parallel} \approx 1.98\text{MHz}$ and $A_{\perp} \approx 0.51\text{MHz}$, yields $\alpha \approx 11.6^\circ$ and $\kappa \approx 0.20$. Although the upper bound on the sequence length is 32, we found that the optimal sequences were much shorter (red crosses). The simulation results indicate that, given a rotation angle θ , the actuator implementation times for rotations around any axis in the $\{\hat{y}, \hat{x}\}$ plane are comparable, with a maximum around $\theta \approx \pi$, and a symmetry for $\theta = \pi \pm \delta$. We plot, in particular, the optimal times $T_A(\theta)$ required to generate the unitaries $X(\theta) \equiv e^{-i\theta\sigma_x/2}$ and $Y(\theta) \equiv e^{-i\theta\sigma_y/2}$ with the actuator scheme (blue circles). Here and in the follow-

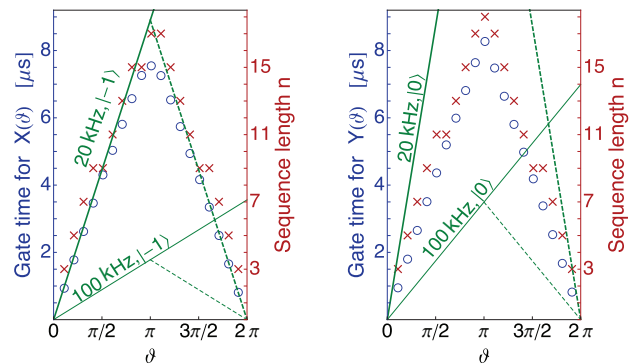


FIG. 1. **Comparison of gate time: Case $\kappa < \cos(\alpha)$** , occurring for a ^{13}C at a distance of $\approx 2.92\text{\AA}$ from the NV center, with an external magnetic field $B_0 \approx 500\text{G}$ aligned with the \hat{z} axis. We plot the simulated actuator implementation time (blue circles-left axis) of the unitaries $X(\theta)$ (left) and $Y(\theta)$ (right) and the corresponding sequence lengths (red crosses-right axis). For comparison, we plot the time required with direct driving (green lines) with bare Rabi frequencies 20 and 100kHz, when the electronic spin in state $|-1\rangle$ (left), thus maximizing the enhancement factor, or $|0\rangle$ (right). Note that the direct-driving time for $\theta > \pi$ depends on whether the driving phase can be inverted (dashed line) or not (solid line).

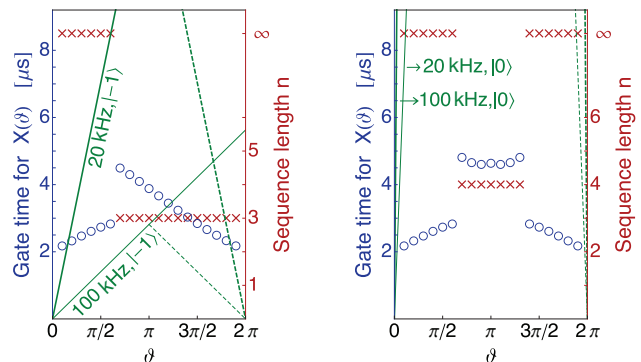


FIG. 2. **Comparison of gate time: Case $\kappa > \cos(\alpha)$** , occurring for a ^{13}C at a distance of $\approx 4.31\text{\AA}$ from the NV center. See Fig. 1 for comparison and explanation of symbols. Note that virtual transition of the electronic spin in the $m_s = 0$ manifold result in a decrease of the effective Rabi frequency, thus making direct driving in that manifold unfavorable.

ing we neglect the time needed for the actuator π -pulses, since it can be as low as 2-5ns [33]. For comparison, we consider direct driving with bare Rabi frequencies in the range $\bar{\Omega} \approx 20\text{--}100\text{kHz}$. In Fig. (1) we plot the gate time $T_D(\theta)$ required with directive driving (green solid and dashed lines), taking into account the Rabi enhancement factors, which for this nuclear spin are $\zeta_0 \approx -2.43$, $\zeta_{+1} \approx 0.62$ and $\zeta_{-1} \approx 1.81$. Note that for bare Rabi frequencies weaker than $\approx 20\text{kHz}$, the actuator protocol is advantageous for any rotation angle.

In Fig. (2), we examine the driving of a ^{13}C at a distance of $\approx 4.31\text{\AA}$ from the NV center, for which $A_{\parallel} \approx$

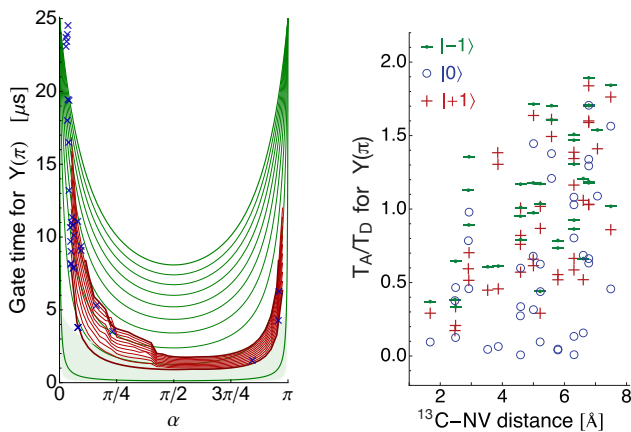


FIG. 3. Left panel: Actuator gate-implementation times for $Y(\pi)$, for the entire α range. Values for κ span from 10^{-3} (bottom thick red line), through 0.1 to 0.9 in 0.1 intervals (thin red lines), to 1 (top thick red line). For the same values of κ , we plot the direct driving times for Rabi frequencies $\Omega \approx 20$ kHz (green lines) and $\Omega \approx 100$ kHz (green shaded region). Blue crosses represent the actuator times for all the tabulated carbon spins around the NV center. Right panel: ratio of actuator to direct driving times for the generation of $Y(\pi)$ in the NV system as a function of the distance between nuclear and electronic spins. We consider all three electronic spin states $|0\rangle$, $|+1\rangle$, $|-1\rangle$ (blue circles, red plus signs, and green dash-dot, respectively), for a bare Rabi frequency $\bar{\Omega} \approx 20$ kHz.

-0.35 MHz and $A_{\perp} \approx 0.23$ MHz. Under the same magnetic field conditions, $B_0 \approx 500$ G, we have $\kappa \approx 1.8$, $\alpha \approx 57.4^\circ$, and thus $\kappa > \cos(\alpha)$, with $n = 6$ the maximal possible length of a finite time-optimal sequence. The figures show the optimal times to synthesize the unitaries $X(\theta)$ and $Y(\theta)$ as a function of the rotation angle θ as well as the corresponding length of the time-optimal sequence. For the synthesis of some unitaries, the optimal scheme requires infinite-length sequences. We compare the time required with the actuator protocol to the direct driving, taking into account the enhancement factors ($\zeta_0 \approx -1.07$, $\zeta_{+1} \approx 0.29$ and $\zeta_{-1} \approx 0.78$). Even if the hyperfine coupling strength is smaller than for the first spin considered, the actuator times are in general smaller; similarly, even for the highest considered direct-driving Rabi frequency the actuator protocol can have a lower time-cost.

While the results shown for particular nuclear spins are indicative of the achievable gate times, the broad range of parameters for different actuator/qubit systems could give rise to quite different behaviors. We thus investigate the actuator implementation time of a particular unitary $Y(\pi)$ for an extended range in $\{\alpha, \kappa\}$ space; the result is plotted in the leftmost panel of Fig. (3). To find the times for a smooth set of parameters, we interpolate the implementation times found numerically for representative pairs $\{\alpha, \kappa\}$. We compare the times achievable with the actuator scheme with the times required for direct driving, taking into consideration the effective Rabi frequencies over the same range of parameters $\{\alpha, \kappa\}$. If only a

moderate driving strength is available (a bare Rabi frequency of $\Omega \approx 20$ kHz) the actuator scheme is faster than direct driving for a broad region of the parameter space. While ^{13}C nuclear spins coupled to the NV center do not span the whole region, other systems might, presenting an even more favorable situation.

As shown in Fig. 3 (right panel), for the NV center system the dependence on the hyperfine parameters of both the actuator scheme time and the direct driving strength yields a broad variation of results for both close-by and more far away nuclei; while a trend toward longer times for the actuator scheme vs. direct driving is apparent as the distance from the NV center increases, the large variations indicate that the best scheme should be evaluated for individual nuclear spins.

Finally, we analyze the effect of the qubit's internal Hamiltonian, which sets the energy gap between its eigenstates. As this increases, the angle α between the two axes of rotation decreases and thus we expect longer sequences (both in terms of number of switches and of total time). On the opposite end, if the energy gap is small, the rotation speeds decrease in both manifolds; thus, although the time-optimal sequences might have short lengths, the total time could still be long. For the nuclear spin qubits, the energy is set by the external magnetic field strength: in Fig. (4) we plot for various fields the bare Rabi frequency for which the actuator implementation time of $Y(\pi)$ coincides with the minimum direct driving time (that is, when the enhancement factor is maximal). If the available experimental bare Rabi frequency is lower than the depicted value at any given field, the actuator control method will yield an advantage over direct driving. At intermediate fields, around $B_0 \approx 250 - 500$ G, Rabi frequencies that favor direct driving are relatively large, indicating a region where actuator control can prove especially beneficial. As before, variations in the hyperfine coupling parameters yield sizeable variations on top of the expected behavior.

Incidentally, the upper bound on the implementation time of any considered unitary, $T \approx 25 \mu\text{s}$, is still much shorter than the nitrogen-vacancy center spin-lattice relaxation time at room temperature, $T_1 \approx 1-10$ ms [21].

III. DISCUSSION

Indirect control of qubits by a quantum actuator is an attractive strategy in many situations when the qubits couple weakly to external fields, but interact more strongly to another quantum system.

Here we analyzed an exemplary situation, consisting of a hybrid quantum register composed of electronic and nuclear spins centered around the NV center in diamond. Using this particular system, we analyzed the parameter space where indirect control by an actuator presents a time-advantage over direct control methods. The comparison was performed by using time-optimal control results. Similar control schemes have been proposed and

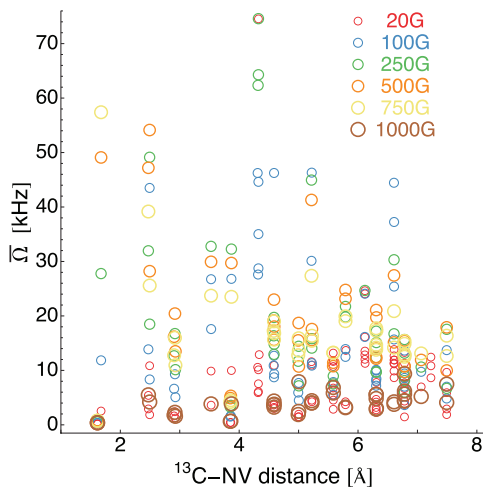


FIG. 4. Minimal bare Rabi frequency for which direct driving is advantageous over the actuator method for the implementation of $Y(\pi)$, for different magnetic fields.

experimentally implemented previously, as it was realized early on that switched control is universal [10, 13]; however, time-optimality was not considered. For example, the most frequent scheme [12, 34, 35] applies alternate rotations for equal times; even if this is a convenient way of implementing dynamical decoupling on the actuator while manipulating the qubits, the scheme is not time-optimal and has in general poor fidelity except in the limit of small qubit/actuator coupling (see appendix D). In contrast, here the electronic spin was used just as an actuator (always in an eigenstate), and as such dynamical decoupling is not required.

An interesting extension of our results would be to *simultaneously* control two or more qubits by the same quantum actuator. While this is possible, provided the qubits are coupled with different strengths [10], it becomes more difficult to find time-optimal solutions except for particular tasks (such as state-to-state transformations [36]) or geometries [2, 37]. Still, even when the goal is to control a larger number of qubits, our results can guide the experimentalist's choice between direct driving and the actuator control, for which these results give an upper bound.

ACKNOWLEDGMENTS

It is a pleasure to thank Boerge Hemmerling, Michele Allegra, Xiaoting Wang and Seth Lloyd for stimulating discussions. We thank Adam Gali for providing us the hyperfine coupling strengths. This work was supported in part by the U.S. Air Force Office of Scientific Research grant No. FA9550-12-1-0292. C.D.A acknowledges support from Schlumberger.

Appendix A: The Nitrogen-Vacancy in diamond

The Nitrogen-Vacancy (NV) center is a localized defect in diamond [38, 39], consisting of a vacancy close to a nitrogen substitutional atom. It is a common impurity in natural diamond and it can be as well created in a controlled manner by nitrogen ion implantation. NV centers have generated much interest thanks to spin-dependent fluorescence, optical polarization and good coherence properties even at room temperature, with applications ranging from sensors to fluorescent biomarkers and qubits.

Single NV centers can be detected by optical scanning confocal microscopy with excitation at 532nm and fluorescence emission in the range 650-800nm. The NV spin state can be measured even at room temperature using spin-dependent decay into metastable states: The $|\pm 1\rangle$ states undergo spin-orbit induced inter-system crossing [40], decaying in $1/3^{\text{rd}}$ of the cases to metastable singlet states (with ~ 300 ns lifetime) followed by non-radiative decay to the ground state. Thus, a NV in the $|0\rangle$ state will emit more photons on average than a NV in the $|\pm 1\rangle$ states, yielding state discrimination by fluorescence intensity. Room temperature optically detected magnetic resonance (ODMR) of a single NV spin was demonstrated in groundbreaking experiments [41, 42]. The metastable state decays via spin-non conserving processes into the $|0\rangle$ state thereby re-orienting the spin. While this reduces measurement contrast, it allows spin polarization in excess of 95%.

The ground state of the NV electronic spin can be manipulated by on-resonance microwave fields. The $|0\rangle$ and $|\pm 1\rangle$ levels are separated by a zero field splitting $\Delta \approx 2.87\text{GHz}$. A small magnetic field aligned with the NV axis splits the degeneracy between the $|\pm 1\rangle$ levels, allowing addressing one transition at a time, as considered in the main text.

NV centers have garnered much attention also due to their very good coherence properties. Coupling to phonons is weak and relaxation is dominated by spin-spin processes. For ultra-pure type II-a diamond, the main source of decoherence is the nuclear ^{13}C spin bath, which can be further suppressed in isotopically engineered diamonds [43–45]. The coherence time can be extended by using dynamical decoupling techniques (a series of π pulses) [46, 47] to $T_2 \approx 600\mu\text{s}$ in natural diamond [20, 48, 49]. The limiting factor is the T_1 relaxation process of NV centers. The process is generally slow thanks to low coupling to phonons yielding relaxation times of $T_1 \approx 5\text{-}10$ ms (depending on the NV and other paramagnetic impurity density).

While the nuclear spin bath is a source of decoherence, proximal individual ^{13}C nuclear spins can be used as a resource [27, 50]. Because ^{13}C isotopic impurities are distributed randomly in the diamond lattice with 1.1% probability, each NV centre couples to spins at different locations, leading to distinct hyperfine structure and coherence properties. We can consider the discrete set of

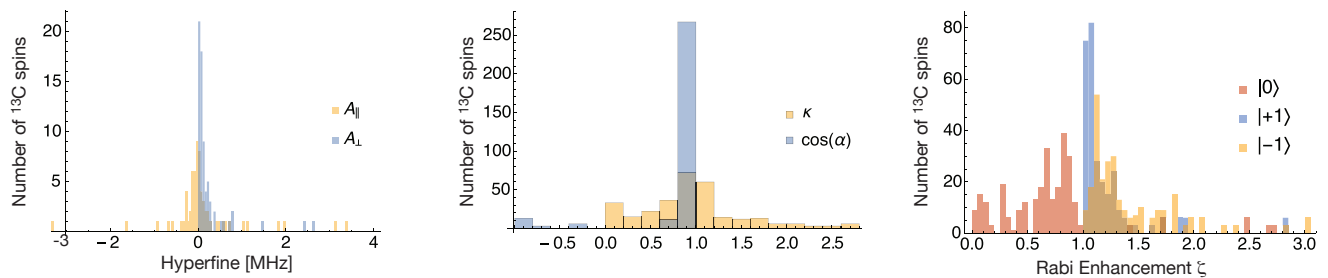


FIG. 5. Left: Histogram of the distribution of hyperfine coupling strengths for the closest 70 nuclear spins. Center: Histogram of the relevant parameters for time-optimal control for the closest nuclear spins calculated from their coupling to a NV center in diamond at $B_0 = 500\text{G}$ using the hyperfine couplings on the left. Right: Histogram of Rabi enhancement factors, $|1 + \zeta_i|$, for the closest nuclear spins to a NV center in diamond at $B_0 = 500\text{G}$. While a few spins have large enhancement > 3 (not plotted), the majority of spins have factors $1 - 1.5$.

proximal lattice sites, in the first five lattice cells, that will be probabilistically occupied by a ^{13}C nuclear spin. The hyperfine coupling of these nuclear spins to the NV center is set by their positions through the dipolar interaction and the contact term, which is set by the NV electronic spin wavefunction density at the spin location. We used the results of ab-initio calculations [29, 32, 51] that yield a discrete set of possible hyperfine splittings for the ^{13}C in the region of interest. Because of the strong angular dependence of the magnetic dipolar coupling and of the electronic wavefunction (which presents a C_{3v} symmetry) there is a wide variety of coupling strengths, even for nuclear spins at similar distances from the central NV electronic spin, leading to different results in the comparison between the quantum and classical control strategies, as discussed in the main text.

Here we thus survey some of the relevant properties for the comparison of direct driving versus the actuator model. We considered the ^{13}C nuclear spin in the first 5 lattice cells around the NV center. As shown in Figure 5, there is a great variation in the hyperfine parameters, even for spins that are located at similar distances from the NV center. This in turns translates into a spread in the enhancement factors of the Rabi driving frequency (right panel) and the magnitude and angle of the axis of rotation in the $m_s = 1$ manifold (left panel).

Appendix B: Enhancement of the Rabi driving

In the qubit/actuator model, a critical assumption is that the actuator can be controlled by an external driving much faster than the qubit. In addition, for the actuator model to have an advantage in terms of gate-implementation time, the actuator-qubit coupling should be strong. Under these conditions, there is a large energy-scale separation between the qubit and the actuator and a careful analysis of their joint dynamics is needed.

In particular, for electronic and nuclear spin systems, the nuclear spin driving field also couple to the electronic spin. While this coupling is well off-resonance, it is in

general quite strong and cannot be disregarded. Because the driving is off-resonant, it cannot induce electronic transitions. However, it can increase the probability of the on-resonance nuclear spin transition probabilities, thanks to virtual transitions. This enhancement has been long observed in ENDOR (electron-nuclear double resonance) experiments [25, 52, 53] and is usually described as a pseudo-Zeeman effect, affecting both the resonance frequency and the transition probability of nuclear spins.

The enhancement is due to the mixing of the nuclear spin Zeeman eigenstates due to the anisotropic hyperfine interaction. We can calculate the enhancement by performing second order perturbation theory in the hyperfine coupling strength, obtaining:

$$\begin{aligned}\zeta_{+1} &= \frac{\gamma_e}{\gamma_n} \frac{2A_{\perp}}{\Delta + B_0(\gamma_e - \gamma_n) - A_{\parallel}}; \\ \zeta_{0} &= -\frac{\gamma_e}{\gamma_n} \frac{4A_{\perp}(\Delta - A_{\parallel})}{(\Delta + B_0(\gamma_e - \gamma_n) - A_{\parallel})(\Delta - B_0(\gamma_e - \gamma_n) - A_{\parallel})}; \\ \zeta_{-1} &= \frac{\gamma_e}{\gamma_n} \frac{2B}{\Delta - B_0(\gamma_e - \gamma_n) - A_{\parallel}}.\end{aligned}\quad (\text{B1})$$

We can rewrite these expressions in terms of the parameters α , κ which determine the performance of the actu-

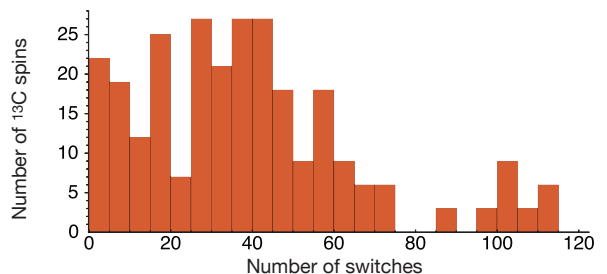


FIG. 6. Maximum number of switches required for the time optimal solution. Here we survey the closest nuclear spins to a NV center in diamond at $B_0 = 500\text{G}$.

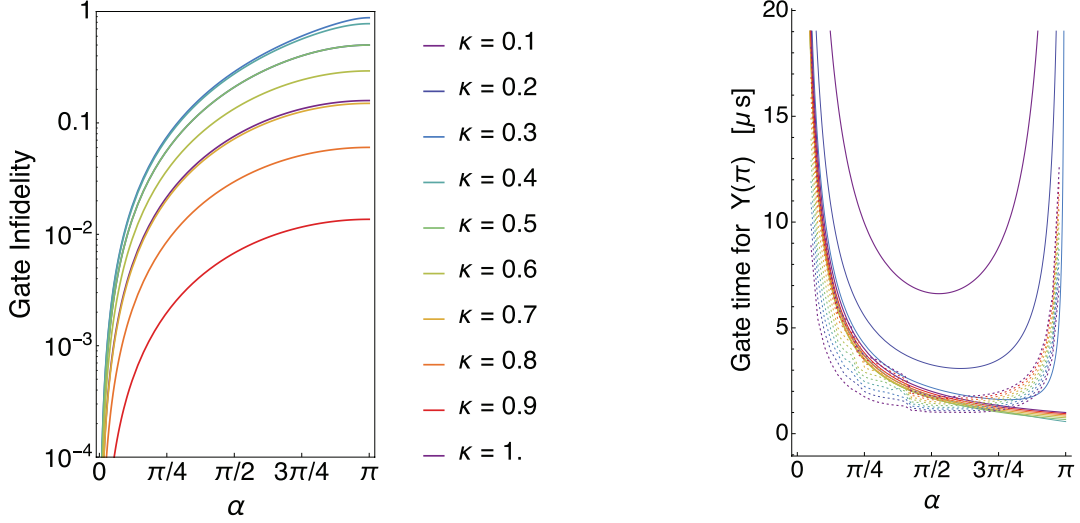


FIG. 7. Left: Gate Infidelity $1 - |\text{Tr}\{U_{eq}U_g^\dagger\}|$, where U_g is a π rotation about Y. Here U_{eq} is obtained by rotations around alternating axes (separated by an angle α) for equal time periods. While the fidelity is good for small α , it becomes poor at larger α . Note that the infidelity for the time-optimal scheme is in principle 0 and was set to $< 10^{-10}$ in the numerical searches. Right: Gate time for the same gate (solid lines) compared to the time-optimal solution time (dotted lines). Note that the equal-time solutions seem to be time-favorable at high α , but then their fidelity is poor.

ator protocol:

$$\begin{aligned}\zeta_{+1} &= \frac{2B_0\gamma_e \sin(\alpha)}{\kappa(B_0\gamma_e + \Delta) - B_0\gamma_n \cos(\alpha)}; \\ \zeta_0 &= -\frac{4B_0\gamma_e \sin(\alpha)(\kappa(B_0\gamma_n + \Delta) - B_0\gamma_n \cos(\alpha))}{[\kappa(B_0\gamma_e + \Delta) - B_0\gamma_n \cos(\alpha)]\{\kappa[\Delta - B_0(\gamma_e - 2\gamma_n)] - B_0\gamma_n \cos(\alpha)\}} \\ \zeta_{-1} &= \frac{2B_0\gamma_e \sin(\alpha)}{\kappa[\Delta - B_0(\gamma_e - 2\gamma_n)] - B_0\gamma_n \cos(\alpha)}.\end{aligned}\tag{B2}$$

Note that the enhancement is proportional to the ratio γ_e/γ_n , which is in general quite large. More generally, this corresponds to a proportionality to the relative coupling strength of the actuator and qubit to external fields.

Note that ζ_i can be either positive or negative, depending on the sign of the transverse hyperfine coupling, thus leading to either an enhancement or a reduction of the effective Rabi frequency $\Omega_i = (1 + \zeta_i)\bar{\Omega}$.

Appendix C: Length of quantum actuator control sequences

While in the main text we neglected the time required to apply π -pulses on the NV center, this time can become substantial if the number of required pulses grows. In addition, pulse errors might also accumulate and degrade the nuclear spin unitary fidelity. The actuator sequence length is thus a very important parameter, and we thus survey in Figure 6 its spread over the nuclear spins of interest. In particular we plot the maximum sequence length, as determined by constraints on the time-optimal solution [23], while the actual solution might be much

shorter.

We note that for typical parameters, the sequence length is relatively short, as good implementation of dynamical decoupling pulse sequences comprising more than thousands π pulses have been implemented, both in the NV spin system [54] and in other systems [55–57], including a long tradition in nuclear magnetic resonance, where thousands of pulses are routinely employed.

Appendix D: Fidelity of quantum actuator control

The simplest scheme to obtain rotations of the target qubit is by alternating its evolution about the two non-parallel axes for equal amounts of time. While this scheme has advantages, in particular when one also seek to preserve the coherence of the quantum actuator [12, 34] or when the exact rotation axes are not known with enough precision, it provides high fidelity gates only for small angles α . In addition, the rotations are not time-optimal. In figure 7 we compare the equal-time sequences with the time-optimal sequences. While the time-optimal construction can achieve in principle perfect fidelity (and we set the infidelity to 10^{-10} in the numerical searches) the equal-time decomposition does not leave enough degrees of freedom to achieve the desired gate. The fidelity is worse for large angles between the rotation axes and a large mismatch between the two rotation rates. When the equal time decomposition achieves acceptable fidelities, this is paid for by long decomposition times.

- [1] S. Lloyd, A. J. Landahl, and J.-J. E. Slotine, *Phys. Rev. A* **69**, 012305 (2004).
- [2] D. Burgarth, K. Maruyama, M. Murphy, S. Montangero, T. Calarco, F. Nori, and M. B. Plenio, *Phys. Rev. A* **81**, 040303 (2010).
- [3] F. Strauch, *Phys. Rev. A* **84**, 052313 (2011).
- [4] K. Jacobs, *Phys. Rev. Lett.* **99**, 117203 (2007).
- [5] P. Rabl, P. Cappellaro, M. V. G. Dutt, L. Jiang, J. R. Maze, and M. D. Lukin, *Phys. Rev. B* **79**, 041302 (2009).
- [6] R. Heule, C. Bruder, D. Burgarth, and V. Stojanović, *Phys. Rev. A* **82**, 052333 (2010).
- [7] D. Burgarth, S. Bose, C. Bruder, and V. Giovannetti, *Phys. Rev. A* **79**, 060305 (2009).
- [8] J. J. L. Morton *et al.*, *Nature* **455**, 1085 (2008).
- [9] J. J. L. Morton *et al.*, *Nat. Phys.* **2**, 40 (2006).
- [10] J. S. Hodges, J. C. Yang, C. Ramanathan, and D. G. Cory, *Phys. Rev. A* **78**, 010303 (2008).
- [11] P. Cappellaro, L. Jiang, J. S. Hodges, and M. D. Lukin, *Phys. Rev. Lett.* **102**, 210502 (2009).
- [12] H. Taminiau, J. Cramer, T. van der Sar, V. Dobrovitski, and R. Hanson, *Nat Nano* **9**, 171 (2014).
- [13] N. Khaneja, *Phys. Rev. A* **76**, 032326 (2007).
- [14] B. C. Gerstein and C. R. Dybowski, *Transient techniques in NMR of solids, an introduction to theory and practice* (Academic, Orlando, Fla., 1985).
- [15] U. Boscain and P. Mason, *Journal of Mathematical Physics* **47**, 062101 (2006).
- [16] U. Boscain and B. Piccoli, *Optimal syntheses for control systems on 2-D manifolds*, Mathématiques & applications (Springer, 2004).
- [17] G. C. Hegerfeldt, *Phys. Rev. Lett.* **111**, 260501 (2013).
- [18] F. Jelezko and J. Wrachtrup, *Physica Status Solidi (A)* **203**, 3207 (2006).
- [19] L. Childress, R. Walsworth, and M. Lukin, *Phys. Today* **67**, 38 (2014).
- [20] L. Childress, M. V. Gurudev Dutt, J. M. Taylor, A. S. Zibrov, F. Jelezko, J. Wrachtrup, P. R. Hemmer, and M. D. Lukin, *Science* **314**, 281 (2006).
- [21] M. W. Doherty, F. Dolde, H. Fedder, F. Jelezko, J. Wrachtrup, N. B. Manson, and L. C. L. Hollenberg, *Phys. Rev. B* **85**, 205203 (2012).
- [22] Y. Billig, *Quantum Inf. Process.* **12**, 955 (2013).
- [23] C. D. Aiello, M. Allegra, B. Hemmerling, X. Wang, and P. Cappellaro, *ArXiv:1410.4975* (2014).
- [24] A. D. Boozer, *Phys. Rev. A* **85**, 012317 (2012).
- [25] Bleaney, in *Hyperfine interactions*, edited by A. Freeman and R. Frankel (Academic Press, 1967) p. 1.
- [26] A. Abragam and B. Bleaney, *Electron Paramagnetic Resonance of Transition Ions* (Oxford University Press, Oxford, 2012) p. 228.
- [27] P. C. Maurer, G. Kucsko, C. Latta, L. Jiang, N. Y. Yao, S. D. Bennett, F. Pastawski, D. Hunger, N. Chisholm, M. Markham, D. J. Twitchen, J. I. Cirac, and M. D. Lukin, *Science* **336**, 1283 (2012).
- [28] N. Sun, Y. Liu, L. Qin, H. Lee, R. Weissleder, and D. Ham, *Solid-State Electronics* **84**, 13 (2013).
- [29] A. Gali, M. Fyta, and E. Kaxiras, *Phys. Rev. B* **77**, 155206 (2008).
- [30] S. Felton, A. M. Edmonds, M. E. Newton, P. M. Martineau, D. Fisher, D. J. Twitchen, and J. M. Baker, *Phys. Rev. B* **79**, 075203 (2009).
- [31] A. Dréau, J.-R. Maze, M. Lesik, J.-F. Roch, and V. Jacques, *prb* **85**, 134107 (2012).
- [32] B. Smeltzer, L. Childress, and A. Gali, *New Journal of Physics* **13**, 025021 (2011).
- [33] G. D. Fuchs, V. V. Dobrovitski, D. M. Toyli, F. J. Heremans, and D. D. Awschalom, *Science* **326**, 1520 (2009).
- [34] G.-Q. Liu, H. C. Po, J. Du, R.-B. Liu, and X.-Y. Pan, *Nature Communications* **4**, 2254 (2013).
- [35] T. W. Borneman, C. E. Granade, and D. G. Cory, *Phys. Rev. Lett.* **108**, 140502 (2012).
- [36] E. Assémat, M. Lapert, Y. Zhang, M. Braun, S. J. Glaser, and D. Sugny, *Phys. Rev. A* **82**, 013415 (2010).
- [37] Y. Zhang, C. A. Ryan, R. Laflamme, and J. Baugh, *Phys. Rev. Lett.* **107**, 170503 (2011).
- [38] F. Jelezko, T. Gaebel, I. Popa, A. Gruber, and J. Wrachtrup, *Phys. Rev. Lett.* **92**, 076401 (2004).
- [39] J. Wrachtrup and F. Jelezko, *J. Phys.: Condens. Matter* **18**, S807 (2006).
- [40] N. B. Manson, J. P. Harrison, and M. J. Sellars, *Phys. Rev. B* **74**, 104303 (2006).
- [41] A. Gruber, A. Drabenstedt, C. Tietz, L. Fleury, J. Wrachtrup, and C. v. Borczyskowski, *Science* **276**, 2012 (1997).
- [42] F. Jelezko, C. Tietz, A. Gruber, I. Popa, A. Nizovtsev, S. Kilin, and J. Wrachtrup, *Single Molecules* **2**, 255 (2001).
- [43] G. Balasubramanian, P. Neumann, D. Twitchen, M. Markham, R. Kolesov, N. Mizuochi, J. Isoya, J. Achard, J. Beck, J. Tissler, V. Jacques, P. R. Hemmer, F. Jelezko, and J. Wrachtrup, *Nat. Mater.* **8**, 383 (2009).
- [44] N. Mizuochi, P. Neumann, F. Rempp, J. Beck, V. Jacques, P. Siyushev, K. Nakamura, D. J. Twitchen, H. Watanabe, S. Yamasaki, F. Jelezko, and J. Wrachtrup, *Phys. Rev. B* **80**, 041201 (2009).
- [45] P. Neumann, R. Kolesov, V. Jacques, J. Beck, J. Tisler, A. Batalov, L. Rogers, N. B. Manson, G. Balasubramanian, F. Jelezko, and J. Wrachtrup, *New J. Phys.* **11**, 013017 (2009).
- [46] E. L. Hahn, *Phys. Rev.* **80**, 580 (1950).
- [47] L. Viola and S. Lloyd, *Phys. Rev. A* **58**, 2733 (1998).
- [48] T. Gaebel, M. Domhan, I. Popa, C. Wittmann, P. Neumann, F. Jelezko, J. R. Rabeau, N. Stavrias, A. D. Greentree, S. Prawer, J. Meijer, J. Twamley, P. R. Hemmer, and J. Wrachtrup, *Nat. Phys.* **2**, 408 (2006).
- [49] J. R. Maze, P. L. Stanwix, J. S. Hodges, S. Hong, J. M. Taylor, P. Cappellaro, L. Jiang, A. Zibrov, A. Yacoby, R. Walsworth, and M. D. Lukin, *Nature* **455**, 644 (2008).
- [50] M. V. G. Dutt, L. Childress, L. Jiang, E. Togan, J. Maze, F. Jelezko, A. S. Zibrov, P. R. Hemmer, and M. D. Lukin, *Science* **316**, 1312 (2007).
- [51] A. Gali, “Private communication.”
- [52] A. Abragam and B. Bleaney, *Electron Paramagnetic Resonance of Transition Ions* (Clarendon Press, Oxford, 1970).
- [53] A. Schweiger and G. Jeschke, *Principles of Pulse Electron Paramagnetic Resonance* (Oxford University Press, 2001).
- [54] N. Bar-Gill, L. Pham, A. Jarmola, D. Budker, and R. Walsworth, *prb* **4**, 1743 (2013).

- [55] M. Ali Ahmed, G. Álvarez, and D. Suter, *Phys. Rev. A* **87**, 042309 (2013).
- [56] M. J. Biercuk, H. Uys, A. P. VanDevender, N. Shiga, W. M. Itano, and J. J. Bollinger, *Nature* **458**, 996 (2009).
- [57] J. Bylander, S. Gustavsson, F. Yan, F. Yoshihara, K. Harrabi, G. Fitch, D. G. Cory, and W. D. Oliver, *Nat. Phys.* **7**, 565 (2011).